Infinite Science Publishing

Proceedings Article

A Deblurring Model for X-space MPI Based on Coded Calibration Scenes

Esen Ergun [a,*] · Abdullah Ömer Arol [a,b] · Emine Ulku Saritas [a,b,c] · Tolga Çukur [a,b,c]

[a]Department of Electrical and Electronics Engineering, Bilkent University, Ankara, Turkey
[b]National Magnetic Resonance Research Center (UMRAM), Bilkent University, Ankara, Turkey
[c]Neuroscience Program, Sabuncu Brain Research Center, Bilkent University, Ankara, Turkey
*Corresponding author, email: esen.ergun@ug.bilkent.edu.tr

Abstract

X-space reconstructions suffer from blurring caused by the point spread function (PSF) of the Magnetic Particle Imaging (MPI) system. Here, we propose a deep learning method for deblurring x-space reconstructed images. Our proposed method learns an end-to-end mapping between the gridding-reconstructed collinear images from two partitions of a Lissajous trajectory and the underlying magnetic nanoparticle (MNP) distribution. This nonlinear mapping is learned using measurements from a coded calibration scene (CCS) to speed up the training process. Numerical experiments show that our learning-based method can successfully deblur x-space reconstructed images across a broad range of measurement signal-to-noise ratios (SNR) following training at a moderate SNR.

I. Introduction

There are two main reconstruction methods in magnetic particle imaging (MPI): system function reconstruction (SFR) and x-space reconstruction. SFR requires calibration measurements from each voxel in the field-of-view (FOV) [1]. These lenghty calibration measurements need to be repeated whenever a scanning parameter or the magnetic nanoparticle (MNP) tracer is changed. One approach to speed up the calibration process is to perform compressed sensing (CS), at the expense of reduced signal-to-noise ratio (SNR) efficiency [2]. A recent study has proposed a coded calibration scene (CCS) with multiple MNP samples distributed in a pseudo-random but connected fashion [3]. Utilizing a CCS instead of a point source sample can simultaneously speed up the calibration process and boost SNR efficiency.

In contrast to SFR, x-space reconstruction does not require calibration measurements, as it directly grids the speed-compensated received signal to the instantaneous location of the field free point (FPP). However, x-space

reconstruction produces blurred images due to the point spread function (PSF) of the imaging system [4].

Here, we introduce a deep-learning model to reduce the blurring in x-space reconstructed images. For practicality, we propose to train the model using a single, realistic CCS with vessel-like structures.

II. Methods and materials

II.I. Numerical Experiments

For model training, we used a CCS of size 7.14×7.14 cm^2 consisting of continuous channels with varying particle concentrations and thicknesses, as shown in Fig. 1a. This CCS is considerably larger than the targeted 2×2 cm^2 FOV. Therefore, distinct MNP distributions can easily be achieved by gradually rotating and sliding the CCS, as proposed in [3]. Following this approach, 3300 distinct measurements were acquired from the CCS, which were divided into training and validation sets as (3000,300).
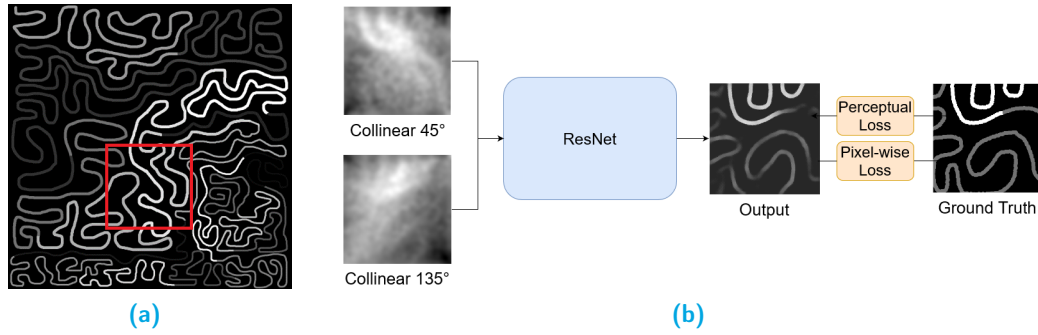
Figure 1: (a) The CCS and (b) the model block diagram. A sample 2×2 cm^2 FOV is marked with the red square. The block diagram shows the 45° and 135° collinear images gridded from the two partitions of the Lissajous trajectory at SNR = 20, the network output and the ground truth MNP distribution. The proposed model is based on a residual neural network (ResNet) backbone trained with pixel-wise and perceptual losses. The network consists of 9 ResNet blocks.
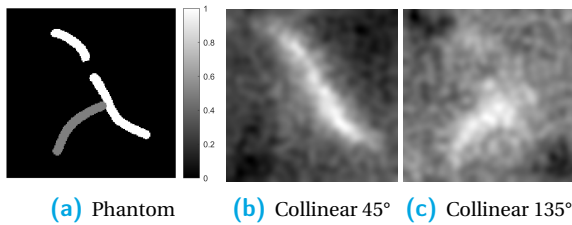

Figure 2: (a) λ-shaped phantom and x-space gridding reconstructions of collinear images from (b) 45° and (c) 135° partitions of the Lissajous trajectory at SNR = 20.

We also used a λ-shaped phantom shown in Fig. 2a to test the performance of the model.

In MPI simulations, selection field gradients of (3, 3, -6) T/m were utilized, together with a Lissajous trajectory with drive field frequencies of 24.75 kHz and 25 kHz along the x- and y-directions, respectively. This trajectory scanned a 2×2 cm^2 FOV, discretized into a 280×280 grid. For image reconstruction, first the Lissajous trajectory was partitioned into two non-overlapping segments corresponding to approximately 45° and 135° scanning angles. For each partition, the virtual collinear coil signal was utilized in an automated gridding reconstruction for non-Cartesian x-space MPI [5].

To analyze the noise performance of the proposed model, additive white Gaussian noise (AWGN) was added at the x- and y- receiver coil signals to maintain SNRs ranging between 5 to 40. At each test SNR level, Monte Carlo simulations with 100 repetitions were performed. SNR was defined as the ratio of the maximum signal intensity during the acquisition of the training data from the entire CCS and the standard deviation of the AWGN.

II.II. Deblurring Model

We devised a deblurring model based on the residual neural network (ResNet) backbone [6] adopted from [7] to deblur x-space reconstructed images (see Figure 1b). The network was trained to minimize pixel-wise ℓ_1 and perceptual losses with equal weights, the latter referring to the ℓ_1-norm distance of activation vectors in the second Visual Geometry Group (VGG) network layer [8] between the model output and the ground truth image. This perceptual loss was adopted since it is suggested to improve realism in image processing tasks [9]. Training the network for 10 epochs on a GeForce RTX 2080 GPU took approximately 20 minutes.

Our model learns an end-to-end mapping from the two partitioned collinear images to the underlying MNP distribution. To achieve a quantitative mapping of the MNP concentration, we normalized the partitioned images in a given pair by the maximum pixel intensity in their average to construct model inputs. The model output was then rescaled back to restore the original intensity range. These pre- and post-scaling steps improved model performance for phantoms with different concentration ranges. The negative pixel intensities of the output image were set to zero, since MNP concentration is non-negative. These operations can be expressed as:

$$X = \frac{[Col_{45}, Col_{135}]}{\max(Col_{45} + Col_{135})/2} \tag{1}$$

$$Y = \max(0, T(X)) \max(Col_{45} + Col_{135})/2 \tag{2}$$

X is the two-channel model input, $T(X)$ is the model output, and Y is the final estimate of MNP distribution.

We trained the model on 3000 distinct measurements acquired from the CCS and evaluated its performance on the λ phantom. For image quality assessment, we utilized the peak signal-to-noise ratio (PSNR) metric:

$$PSNR = 10\log_{10} \frac{MN \max(I)^2}{\sum_{k=1}^{M} \sum_{l=1}^{N} (I_{k,l} - Y_{k,l})^2} \tag{3}$$

Here, I is the ground truth MNP distribution, and M and N denote image dimensions.
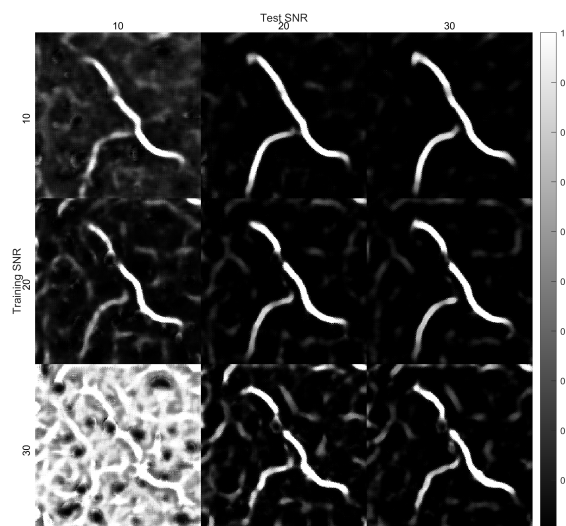
Figure 3: Model output for the λ phantom at various training (rows) versus test (columns) SNR levels.

Figure 4: Noise robustness of the proposed model as a function of training and test SNRs. Mean PSNR for the λ phantom is displayed as a color map for Monte Carlo simulations with 100 repetitions at each test SNR level. PSNR for the noise free case is also displayed for reference.

III. Results & Discussion

Figure 3 shows representative reconstructions at various training and test SNR levels. A main difference between the training CCS and the λ phantom is that the MNP distribution in the phantom is considerably sparse with broad background regions. As a result, a model over-fit to the CCS tends to predict channel-like structures in the background. In particular, the model trained at SNR = 30 generates a considerable amount of artifacts. Moreover, the high-SNR model generalizes poorly to SNR = 10, as it expects low noise levels and is therefore likely to mistake noise for a structure. Model training at lower SNRs helps mitigate both problems: The model trained at SNR = 10 produces substantially lower background artifacts, and shows improved generalization performance. Figure 3 also shows that the model trained at SNR = 10 is unable to recover the disconnected part near the top of the λ phantom. In addition, at all SNR levels, the forking structure of the λ phantom is slightly disconnected. This artifact is likely due to the lack of such a forking structure in the CCS and could be improved by modifying the CCS.

Figure 4 illustrates the noise robustness of the proposed model as a function of training and test SNR levels. Our results indicate that models trained at moderate SNR levels (preferably SNR $\approx$ 10-15) more reliably generalize across noise levels. Furthermore, it is beneficial to use a training SNR that is relatively lower than the test SNR.

IV. Conclusion

In this work, we proposed a deep-learning model to deblur MPI images in x-space reconstructions. This model is trained using a CCS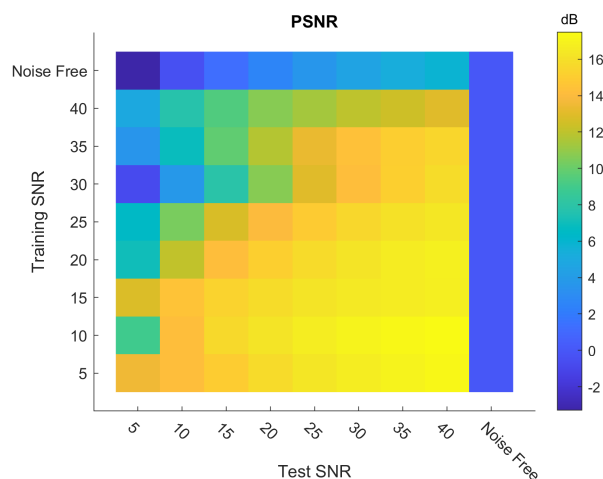 to facilitate measurements for the training procedure. The noise robustness analysis of the proposed method reveals that the model should be trained with noisy images, at SNR levels around 10-15.

Acknowledgments

Author's statement

Conflict of interest: Authors state no conflict of interest.

References

[1] B. Gleich and J. Weizenecker. Tomographic imaging using the nonlinear response of magnetic particles. *Nature*, 435:1214–7, 2005, doi:10.1038/nature03808.

[2] T. Knopp and A. Weber. Sparse reconstruction of the magnetic particle imaging system matrix. *IEEE Transactions on Medical Imaging*, 32(8):1473–1480, 2013, doi:10.1109/TMI.2013.2258029.

[3] S. Ilbey, C. B. Top, A. Güngör, T. Çukur, E. U. Saritas, and H. E. Güven. Fast system calibration with coded calibration scenes for magnetic particle imaging. *IEEE Transactions on Medical Imaging*, 38(9):2070–2080, 2019, doi:10.1109/TMI.2019.2896289.

[4] P. W. Goodwill and S. M. Conolly. Multidimensional x-space magnetic particle imaging. *IEEE Transactions on Medical Imaging*, 30(9):1581–1590, 2011, doi:10.1109/TMI.2011.2125982.

[5] A. Ozaslan, A. Alacaoglu, O. Demirel, T. Cukur, and E. Saritas. Fully automated gridding reconstruction for non-cartesian x-space magnetic particle imaging. *Physics in Medicine and Biology*, 64, 2019, doi:10.1088/1361-6560/ab3525.

[6] K. He, X. Zhang, S. Ren, and J. Sun, Deep residual learning for image recognition, 2015. arXiv:1512.03385 [cs.CV].

[7] S. U. Dar, M. Yurt, L. Karacan, A. Erdem, E. Erdem, and T. Çukur. Image synthesis in multi-contrast mri with conditional generative adversarial networks. *IEEE Transactions on Medical Imaging*, 38(10):2375–2388, 2019, doi:10.1109/TMI.2019.2901750.

[8] K. Simonyan and A. Zisserman, Very deep convolutional networks for large-scale image recognition, 2015. arXiv: 1409.1556 [cs.CV].

[9] C. Ledig, L. Theis, F. Huszar, J. Caballero, A. Cunningham, A. Acosta, A. Aitken, A. Tejani, J. Totz, Z. Wang, and W. Shi, Photo-realistic single image super-resolution using a generative adversarial network, 2017. arXiv: 1609.04802 [cs.CV].